Food Packaging and Shelf Life 55 (2026) 101769

Contents lists available at ScienceDirect

Food Packaging and Shelf Life

journal homepage: www.elsevier.com/locate/fpsl

Protective performance of a composite packaging for kiwifruit under simulated express transport and variable environmental conditions

Jie Hao [a,b,*], Zhinan Wu [a], Hao Liu [c], Yun Yang [a], Minggang Wang [a], Clément Burgeon [b], Marie-Laure Fauconnier [b]

[a] College of Mechanical and Electronic Engineering, Northwest A&F University, Yangling, Shaanxi 712100, China
[b] Laboratory of Chemistry of Natural Molecules, University of Liège, Gembloux Agro-Bio Tech. 2, Passage des Déportés, Gembloux B-5030, Belgium
[c] People's Government of Jigesta Town, Ordos City, Inner Mongolia Autonomous Region 014300, China

ARTICLE INFO

Keywords:
Kiwifruit
CT-NU composite packaging
Temperature and relative humidity
Finite element simulation
Compression

ABSTRACT

This study aims to assess the efficacy of the CT-NU packaging system, which combines corrugated cardboard boxes and expandable polyethylene (EPE) foam packaging nets, in preventing mechanical damage to kiwifruit during transport within express delivery. The protective performance of the composite packaging under top and side-load compression was thoroughly analyzed, considering varying temperature conditions (1, 21, and 40℃) and relative humidity (RH) levels (40%, 60%, and 80%). Experiments were conducted to determine the mechanical properties of both the packaging materials and kiwifruit under different environmental conditions, leading to the development and validation of a three-dimensional finite element model (FEM). The results indicated at a compression depth of 15 mm, the peak local stress in the kiwifruit exceeded 0.35 MPa during the top-load compression simulation and surpassed 0.4 MPa during the side-load compression simulation, both of which under the simulated compression conditions exceeded the fruit's damage threshold. The compression depth and the modulus of elasticity of the corrugated board are critical factors influencing the maximum compressive force and stress in corrugated boxes. The developed regression models for top-load compression ($R^2 > 0.85$) and side-load compression ($R^2 > 0.79$) demonstrate a high level of accuracy in predicting the system's mechanical response. Damage to kiwifruit arises from the combined effects of multiple factors, including the maximum stress, maximum compressive force, compression depth, and the elastic modulus of both the corrugated cardboard box and the EPE foam packing nets. This study lays the foundation for optimizing packaging design and minimizing mechanical damage during transportation, integrating experimental validation with finite element simulation.

1. Introduction

Kiwifruit holds a significant position in the global premium fruit market due to its distinctive nutritional, economic, and health benefits (Lin et al., 2024). It is predominantly consumed fresh. Kiwifruit are susceptible to mechanical damage throughout the supply chain, leading to bruising, deformation, or even rotting of the fruit (Hao et al., 2025; Opara & Pathare, 2014). As a critical element of the kiwifruit supply chain, composite packaging plays a key role in maintaining the integrity and quality of the fruit during transportation and storage by preventing damage and loss (Palsson & Sandberg, 2021; Lin et al., 2023). Therefore, exploring the damage-prevention capabilities of kiwifruit composite packaging is vital for refining its design and production processes, enhancing its protective performance, and minimizing fruit losses across the supply chain. This ultimately reduces transportation costs and boosts profitability.

Compressive forces often occur when fruit is stacked or comes into contact with packaging containers, easily resulting in localized bruising (Yu et al., 2024; Li & Thomas, 2014). Finite element model (FEM) and comparative experiments have been used to assess the effectiveness of various packaging types in reducing mechanical damage to fruit. Previous studies have evaluated various packaging types (e.g., expanded polystyrene, EPE foam nets, ventilated corrugated boxes) for fruit protection, identifying key factors such as material modulus, vent design, and structural geometry (Xia et al., 2020; An et al., 2023; Ambaw et al., 2022; Opara & Fadiji, 2018; Fadiji, Coetzee & Pathare, & Opara, 2016).

* Corresponding author at: College of Mechanical and Electronic Engineering, Northwest A&F University, Yangling, Shaanxi 712100, China.
E-mail address: nx_haojie@163.com (J. Hao).

https://doi.org/10.1016/j.fpsl.2026.101769
Received 3 February 2026; Received in revised form 23 April 2026; Accepted 6 May 2026
Available online 14 May 2026

Fernando et al. (2018) indicated that the one-piece corrugated box provides optimal mechanical cushioning protection for bananas. Fadiji, Coetzee, and Opara (2016) observed that bulk packing led to bruising rates more than 50% higher than those of layered packing during apple transport, with fruit at the bottom being particularly vulnerable to damage. However, most research focuses on assessing fruit damage under single packaging formats or load types, while systematic investigations into the overall response of composite packaging under complex compressive loads are still lacking (Xia et al., 2020). Moreover, real transport involves fluctuating temperature and humidity, which alter material mechanical properties and cushioning performance, an aspect largely overlooked in previous studies (Marin et al., 2021; Csavajda & Böröcz, 2021; Yu et al., 2025a). In particular, the protective performance of CT-NU composite packaging (corrugated box combined with EPE foam nets) under top-load and side-load compression has not been systematically evaluated.

This study investigates the commercially prevalent CT-NU kiwifruit packaging system. By experimentally determining the mechanical properties of its constituent materials (corrugated cardboard, EPE foam packaging nets, and kiwifruit) under varying temperature and humidity conditions, a three-dimensional FEM was developed and validated. The specific objectives of this study were: (1) to simulate the mechanical responses of CT-NU composite packaging under both top-load and side-load compression using a validated 3D FEM, and to compare the damage patterns under the two loading modes; (2) to quantify how temperature (1–40℃) and relative humidity (40–80% RH) affect the elastic moduli of corrugated board, EPE foam nets, and kiwifruit, and thereby influence the system's compressive behavior; (3) to establish regression models that predict maximum compressive force and fruit stress, identifying the key factors (e.g., compression depth, material modulus) that dominate fruit damage risk. This study contributes to the design and development of damage resistant packaging for kiwifruit, helping to reduce mechanical damage during transport and extend the fruit's shelf life. Fig. 1 showed the experimental setup and workflow for evaluating the mechanical damage protection of CT-NU packaging on kiwifruit.

2. Materials and methods

2.1. Sample Preparation

The kiwifruit composite packaging currently prevalent in the market consists of a corrugated cardboard box and EPE foam packaging nets (Fig. 1A). This type of kiwifruit packaging is designated as CT-NU in accordance with the national standard GB/T16472–2013 and the European Union Recommendation No. 21. The corrugated cardboard box is a foldable type (one-piece box), made of double-wall corrugated cardboard (five layers of paper, with the inner liner, fluting, and outer liner bonded using 160, 140, and 110 g/m^2 corrugated paper, respectively), with a BE flute profile. The design is intended to hold 2.5 kg of kiwifruit. The kiwifruit were of the *Cuixiang* variety.

2.2. Determination of mechanical parameters of packaging systems

Corrugated cardboard and EPE foam nets were considered isotropic. The complete CT-NU packaging-kiwifruit system comprises over 3.1 million elements (mentioned in Section 2.3.1), and adopting anisotropic constitutive models would substantially increase computational cost and cause convergence difficulties, exceeding the acceptable scope of engineering simulation. Furthermore, the primary objective of this study is to evaluate the macro-level force-displacement behavior of the packaging system and the peak stress evolution in the fruit, rather than the microstructural failure mechanisms of the materials. Therefore, within the limits of engineering accuracy, the isotropic assumption is considered reasonable and feasible (Słupska et al., 2026; Lang & Su, 2022; Li et al., 2018; Zhu et al., 2024; Kalita et al., 2021). Ten samples of each material were prepared for each environmental condition, paperboard 100 × 10 mm and foam nets 75 mm long. Thickness and diameter were measured with a 0.01 mm digital caliper. Mechanical properties of paperboard and foam nets were measured according to GB/T 12914 2018 and GB/T 21143 2014 using a texture analyzer (Universal TA, Tengbainstrument Technology Co., Ltd., China), using methods similar to that reported by An et al. (2023) and Fadiji et al. (2018). Samples were conditioned in a constant temperature and humidity chamber (0–60℃, 0–100% RH) for 24 h before testing. Nine temperature-humidity combinations were used (1, 21, 40℃ and 40%, 60%, 80% RH, Honuo Instrument Co., Ltd., Tianjin, China). Samples were clamped at both ends (paperboard 80 mm, foam 55 mm) and stretched at 0.17 mm·s^{-1} until fracture to obtain force-displacement curves. The mechanical parameters were calculated using the following formula (Yang et al., 2024; Yu et al., 2025b). The equivalent elastic modulus of paperboard was calculated following Meng (2010).

$$\sigma_y = \frac{F_{\max}}{A} \tag{1}$$

$$\varepsilon_y = \frac{\Delta L}{L} \tag{2}$$

$$\mathrm{E} = \frac{\sigma_y}{\varepsilon_y} \tag{3}$$

$$E_e = \frac{\sum_{i=1}^{n} E_{fyi} t_i + \sum_{j}^{m} c_j E_{cyj} t_{cj}}{H} \tag{4}$$

where σ_y is the fracture stress, F_{max} is the maximum tensile force, A is the fracture cross-sectional area, ε_y is the fracture strain, ΔL is the elongation of the fracture strain, L is the initial distance between the grips, E is the modulus of elasticity, E_e is the equivalent modulus of elasticity of the multi-layer corrugated board, E_{fyi} is the equivalent modulus of elasticity of the i^{th} layer of linerboard, t_i is the thickness of the i^{th} layer of linerboard, c_j is the unfolding coefficient of the j^{th} layer of core paper, E_{cyj} is the equivalent modulus of elasticity of the j^{th} layer of core paper, t_{cj} is the thickness of the j^{th} layer of core paper, and m is the number of layers of core paper.

For each combination of temperature and humidity, 10 kiwifruit samples were tested for elastic modulus, and another 10 whole fruits were tested for failure stress. All values are reported as mean ± standard deviation (SD). The methods for measuring the mechanical properties of kiwifruit follow those outlined by Liu et al. (2022). Ninety fresh *Cuixiang* variety kiwifruits were hand-picked. Using the method for measuring the mechanical properties of tomatoes at 1℃ and 60% relative humidity (RH) as a reference, 10 standard rectangular kiwifruit samples (60 mm × 8 mm) were prepared using a custom-made double-blade cutter. These samples were immediately placed in a constant temperature and humidity chamber set to 1℃ and 60% RH for 0.5 h of storage. Each sample was promptly placed on a texture analyzer to measure its elastic modulus and breaking stress. To simulate the effects of temperature and humidity on kiwifruit during storage, the storage duration for all experimental samples was uniformly set to 1 h. This duration was based on findings from Alique et al. (2005), which demonstrated that the temperature of cherry pulp could decrease from 40℃ to 1℃ in just 6 min, highlighting that storage time is a critical factor influencing temperature gradients within fruit pulp. During tensile testing, an A/TG probe was used, with the test speed set at 1 mm/s.

Besides, the failure stress of kiwifruit (the stress threshold for mechanical damage) was measured using a compression test. Ninety fresh Cuixiang variety kiwifruits were hand-picked. Whole kiwifruit of similar size (transverse diameter 54 ± 2 mm, longitudinal length 75 ± 3 mm) were selected and compressed using the same texture analyzer equipped with a flat plate probe (diameter 50 mm) at a constant speed of 1 mm/s until visible cracking or 30% deformation. This value was used as the damage criterion in the finite element simulations. This approach of using experimentally determined failure stress as a damage criterion in

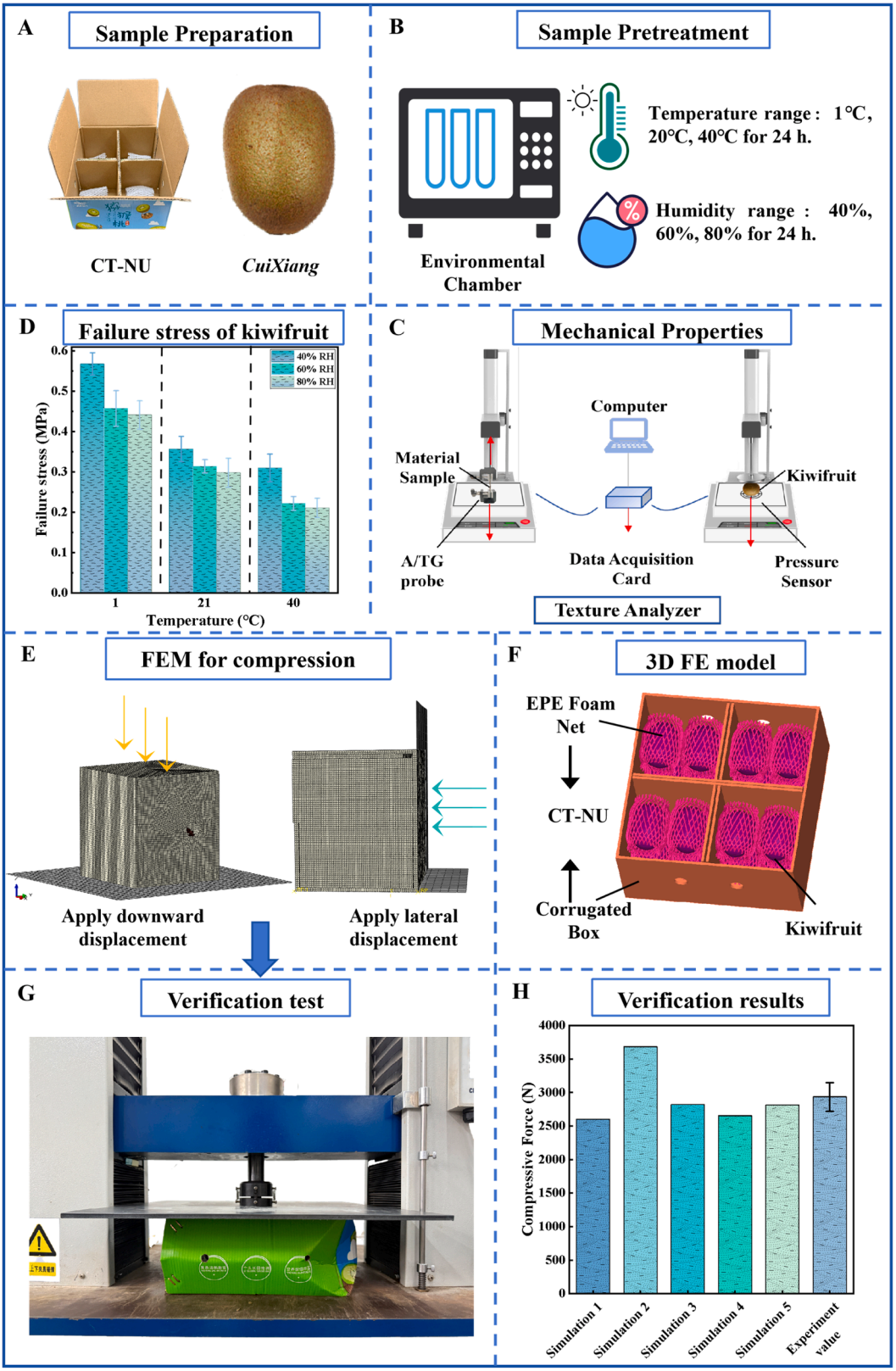

Fig. 1. Experimental setup and workflow for evaluating the mechanical damage protection of CT-NU packaging on kiwifruit. A, Preparation of CT-NU packaging and kiwifruit; B, Sample pretreatment; C, Determination of mechanical properties of kiwifruit and CT-NU materials; D, Measurement of kiwifruit failure stress; E, Construction of the CT-NU-kiwifruit model; F, 3D model compression FEM simulation; G, Compression validation test; H, Comparison of compression test results with simulation results. Note: The failure stress of kiwifruit (0.2–0.7 MPa) used as the damage criterion in the simulations was obtained from independent compression tests on whole fruit, as described in Section 2.2 and illustrated in Fig. 1D.

FEM simulations is adopted in fruit mechanical damage studies (An et al., 2023).

2.3. Analysis of the damage resistance of kiwifruit with the CT-NU packaging system

2.3.1. 3D composite packaging-fruit model and simulation

Step 1: In this step, the 3D models of the composite packaging and kiwifruit were established. The structure of each component was simplified. The kiwifruit had a transverse diameter of 54 mm and a longitudinal length of 75 mm. The corrugated cardboard box measured 270 mm × 255 mm × 130 mm. The foam packaging nets had a diameter of 54 mm and a height of 89 mm, and consisted of foam strips 2.2 mm in diameter arranged in two bonded, interlocking layers, with each layer comprising 25 foam strips. The 3D models of the above components were created in SolidWorks software (Dassault Systems SIMULIA Corp., USA) using simplified dimensions. The interior of the packaging box consists of four storage compartments of identical dimensions. Accordingly, the simulation assumes that all four compartments and the enclosed kiwifruit experience identical loading conditions. The packaging box was divided into four equal sections, and one section (containing four kiwifruit wrapped in foam packaging nets) was selected for subsequent mesh generation. Ground components were created in Abaques software (Dassault Systems SIMULIA Corp., USA).

Step 2: Mesh generation and material property definition were conducted for the corrugated cardboard box, foam packaging nets, and kiwifruit. The segmented packaging box, foam packaging nets, and kiwifruit models were imported into HyperMesh (Altair Corporation, USA). Hexahedral elements (C3D8R) with a mesh size of 1.0 mm were employed for the kiwifruit and corrugated cardboard box. For the EPE foam packaging nets, second-order tetrahedral elements (C3D10M) were generated with a mesh size of 0.15 mm. The packaging system comprising corrugated cardboard boxes, foam nets, and kiwifruit generated a total of 3142,914 units. The packaging system was then imported into Abaques for assembly. The ground surface was meshed in Abaqus using quadrilateral shell elements (S4R). A global mesh size of 0.15 mm was applied, resulting in a total of 100 elements. Based on the mechanical parameters obtained from experiments, the material properties of the corrugated cardboard box, foam packaging nets, and kiwifruit were defined for subsequent simulations.

2.3.2. Validation of the FEM

To validate the accuracy of the proposed 3D FEM model for kiwifruit compression, the simulation results were compared with experimental data. Compression tests were performed on CT-NU composite packaging filled with *Cuixiang* kiwifruit at 30 °C and 70% RH. Specifically, the maximum compressive force predicted by the 3D FEM simulation was compared with the maximum compressive force measured in the physical compression tests of the CT-NU composite packaging containing kiwifruit.

2.3.2.1. Compression method of CT-NU composite packaging-fruit. To validate the accuracy of the FEM predictions for the compression resistance of kiwifruit composite packaging, a comparative experiment was designed and conducted. The test was performed using a DDL10–3365 electronic universal testing machine (Changchun Academy of Science & Technology Co., Ltd., China). Compressive loading was applied to the packaging structure through two rigid plates positioned at the top and bottom. A displacement-controlled loading mode was adopted, with a loading rate of 0.15 mm/s and a maximum compression displacement of 15 mm, thereby simulating the vertical pressure that may occur during actual transportation or stacking. The test environment was maintained under standard laboratory conditions at a temperature of 21 ± 1℃ and 70 ± 5% RH. All samples of corrugated board, EPE foam nets, and kiwifruit were conditioned in the same constant temperature and humidity chamber for 24 h prior to testing to ensure uniform moisture and temperature equilibrium across materials. Five sample groups were selected, each comprising a complete composite packaging structure (including a corrugated cardboard box, foam packaging nets, and fresh kiwifruit). Within each group, fruits were selected such that variations in weight and size did not exceed ±5%. The packaging method was consistent with that used in the simulation model, thereby ensuring uniformity in geometric, material, and structural conditions. Load-displacement curves were recorded using TestXpert 4.0 software (ZwickRoell, Ulm, Germany), and the deformation patterns of the packaging structures were observed and documented photographically. To ensure data comparability, all experiments were conducted identical operational procedures, with force sensors calibrated prior to testing. The maximum compressive force from the physical compression tests was determined as the average value across replicates.

2.3.2.2. Simulation method for compression of CT-NU composite packaging-fruit. Simulation results for three temperature levels at 80% RH and 15 mm displacement, as well as for three RH levels at 21°C and 15 mm displacement, were compared with validation tests. Each condition is denoted using the format *temperature-RH-displacement* (e.g., 21–80–15 represents 21℃, 80% RH, and 15 mm displacement). Across these scenarios, five simulation sets were analyzed. The same notation is used throughout this study. In the CT-NU composite packaging-fruit model, the mechanical parameters of the corrugated cardboard box, foam packaging nets, and kiwifruit corresponding to the five specified gradients were applied. The simulation was conducted with a loading rate of 0.15 mm/s, a compression depth of 15 mm, and a total duration of 100 s. The maximum compressive force was extracted from the simulation results. By comparing the maximum compressive forces obtained from the experiments and simulations, the accuracy of the CT-NU composite packaging-fruit compression system was evaluated.

2.3.3. Loading and simulation

The analysis step was established and boundary conditions were defined. Simulations were conducted using a rigid plate subjected to top-load compression and lateral compression applied in both horizontal and vertical directions, which were treated as two separate simulations. A dynamic analysis step was implemented with geometric nonlinearity enabled. The total analysis duration was set to 100 s, and compression depths of 5 mm, 10 mm, and 15 mm were specified. Material mechanical properties were assigned according to different temperature (1, 21, and 40°C) and RH (40%, 60%, and 80%) conditions, as detailed in Table 1. For the geometric model of the CT-NU composite packaging-fruit compression system, no additional boundary conditions were applied to the packaging or fruit components because the loading was applied via rigid plates moving in displacement control, and all components were free to move in response to contact forces. Only the ground plate was fully constrained. The non-uniform mesh distribution means that excessively small mesh sizes would increase computation time, as the time increments are determined by the smallest mesh features. To improve computational efficiency and accommodate the non-uniform mesh, mass scaling was applied with a target time increment of 1×10^{-6} s to maintain computational stability

The interactions among the CT-NU composite packaging, fruit, and ground geometric models were defined. For contact properties, normal behavior was modeled using hard contact to prevent interpenetration with minimal compliance, while tangential behavior employed penalty friction for its robustness in handling complex multi-surface interactions. These contact properties were specified for each component with isotropic friction behavior. The friction coefficients were determined from separate pilot tests using a custom inclined-plane setup. The friction coefficient between the ground and the corrugated box was set to 0.50, between the EPE foam packaging nets and the corrugated box to

Table 1
Mechanical parameters of the 3D FE model for CT-NU composite packaging material and fruit used in compression damage analysis.

Number	T (℃)	H (%)	E_{Kiwi} (MPa)	E_{EPE} (MPa)	E_{CB} (MPa)	D (mm)	Cited parameters
1	1	40	2.453	0.586	390.619	5	$\rho_{Kiwi} = 1.224$,
2						10	$\rho_{EPE} = 0.024$,
3						15	$\rho_{CB} = 0.204$,
							$\nu_{Kiwi} = 0.30$,
							$\nu_{EPE} = 0.10$,
							$\nu_{CB} = 0.34$
4		60	2.362	0.577	306.036	5	$\rho_{Kiwi} = 1.239$,
5						10	$\rho_{EPE} = 0.023$,
6						15	$\rho_{CB} = 0.193$,
							$\nu_{Kiwi} = 0.30$,
							$\nu_{EPE} = 0.10$,
							$\nu_{CB} = 0.34$
7		80	2.265	0.568	242.463	5	$\rho_{Kiwi} = 1.276$,
8						10	$\rho_{EPE} = 0.023$,
9						15	$\rho_{CB} = 0.188$,
							$\nu_{Kiwi} = 0.30$,
							$\nu_{EPE} = 0.10$,
							$\nu_{CB} = 0.34$
10	21	40	2.306	0.570	408.192	5	$\rho_{Kiwi} = 1.179$,
11						10	$\rho_{EPE} = 0.023$,
12						15	$\rho_{CB} = 0.201$,
							$\nu_{Kiwi} = 0.30$,
							$\nu_{EPE} = 0.10$,
							$\nu_{CB} = 0.34$
13		60	2.243	0.563	296.947	5	$\rho_{Kiwi} = 1.190$,
14						10	$\rho_{EPE} = 0.022$,
15						15	$\rho_{CB} = 0.191$,
							$\nu_{Kiwi} = 0.30$,
							$\nu_{EPE} = 0.10$,
							$\nu_{CB} = 0.34$
16		80	2.159	0.557	274.034	5	$\rho_{Kiwi} = 1.197$,
17						10	$\rho_{EPE} = 0.022$,
18						15	$\rho_{CB} = 0.186$,
							$\nu_{Kiwi} = 0.30$,
							$\nu_{EPE} = 0.10$,
							$\nu_{CB} = 0.34$
19	40	40	2.216	0.548	368.621	5	$\rho_{Kiwi} = 1.122$,
20						10	$\rho_{EPE} = 0.022$,
21						15	$\rho_{CB} = 0.199$,
							$\nu_{Kiwi} = 0.30$,
							$\nu_{EPE} = 0.10$,
							$\nu_{CB} = 0.34$
22		60	2.051	0.534	356.987	5	$\rho_{Kiwi} = 1.134$,
23						10	$\rho_{EPE} = 0.021$,
24						15	$\rho_{CB} = 0.190$,
							$\nu_{Kiwi} = 0.30$,
							$\nu_{EPE} = 0.10$,
							$\nu_{CB} = 0.34$
25		80	1.851	0.528	301.284	5	$\rho_{Kiwi} = 1.165$,
26						10	$\rho_{EPE} = 0.021$,
27						15	$\rho_{CB} = 0.183$,
							$\nu_{Kiwi} = 0.30$,
							$\nu_{EPE} = 0.10$,
							$\nu_{CB} = 0.34$

Note: T - environmental temperature, ℃; H - relative humidity, %; E_{Kiwi} - the elastic modulus of kiwifruit, E_{EPE} - the elastic modulus of EPE foam packing net material, E_{CB} - the elastic modulus of corrugated board, D - the depth of compression, ρ_{Kiwi} - density of kiwifruit, ρ_{EPE} - density of EPE foam packing net material, ρ_{CB} - density of corrugated board, ν_{Kiwi} - Poisson's ratio of kiwifruit, ν_{EPE} - Poisson's ratio of EPE foam packing net material, ν_{CB} - Poisson's ratio of corrugated board.

0.50, and between the kiwifruit and the EPE foam packaging nets to 0.40. In addition, the pressure plate was configured to contact either the top surface (top-load compression) or the side surface (side-load compression) of the package, with contact properties assigned and a friction coefficient of 0.1. Interactions between the remaining surfaces were defined using the display universal algorithm, with the contact property set to all with self. Rigid body constraints were applied to the ground surface, fully fixing all of its degrees of freedom, as its stiffness exceeds that of the corrugated board by more than three orders of magnitude, making its deformation negligible. A structural coupling constraint was established at the top of the corrugated box to simulate the effect of the sealant.

Loading and simulation were carried out with the bottom surface of the rigid ground plate fully constrained in all degrees of freedom. The upper and lateral loading plates, treated as rigid bodies, applied vertical (top) and lateral (side) compressive loads, respectively, in displacement-controlled mode. The simulation used the quasi-static analysis step in ABAQUS 2022, with automatic time increment control enabled and a damping factor of 0.001 to improve convergence stability.

2.4. Statistical analysis

All test results were analyzed using SPSS, with the significance level set at $p = 0.05$. Environmental temperature, RH, compression depth, the elastic modulus of corrugated cardboard boxes, the elastic modulus of EPE foam packaging nets, and the elastic modulus of kiwifruit were selected as independent variables. The dependent variables included two indicators reflecting the damage level of the corrugated cardboard boxes, namely maximum compressive force and maximum stress, and an indicator representing compressive damage to the kiwifruit, specifically maximum stress. Pearson correlation analysis was used to preliminarily assess the strength of the linear relationships between each continuous variable (temperature, relative humidity, compression depth, and various elastic modulus) and each dependent variable (maximum compressive force, maximum stress of the corrugated box, and maximum stress of the kiwifruit), and the correlation coefficients were calculated. Given the potential multicollinearity among the independent variables (temperature, relative humidity, compression depth, and various elastic moduli) and the intercorrelations among the dependent variables (maximum compressive force, maximum stress of the corrugated box, and maximum stress of the kiwifruit), a partial least squares regression (PLSR) model was constructed for prediction. PLSR extracts latent components that simultaneously explain the variance in both independent and dependent variables, thereby overcoming the limitations of traditional multiple linear regression with respect to collinearity (Hao et al., 2023). Variable importance in projection (VIP) was used to assess the contribution of each variable, with VIP > 1 indicating a significant contribution to the model. The direction and relative magnitude of the effect of each independent variable on the dependent variables were presented using standardized regression coefficients (Beta coefficients).

The overall significance of the covariance model was evaluated using an F-test, while the significance of individual model parameters was assessed using t-tests. The figures were generated using Origin 2025b, the three-dimensional models were constructed in SolidWorks 2022, and the finite element simulations were performed in ABAQUS 2022.

3. Results and discussion

3.1. Mechanical properties of kiwifruit and packaging materials

Fig. 2 showed the variation in elastic modulus of corrugated cardboard components under different temperature and humidity conditions. Fig. 2A-D showed that the elastic modulus of all corrugated board components decreased with increasing humidity at constant temperature. This decrease is likely due to higher equilibrium moisture content (EMC) weakening fiber hydrogen bonds (Lin et al., 2022; Allaoui et al., 2009). The elastic modulus exhibited nonlinear variations with temperature. At 40% RH, the elastic modulus first increased and then decreased with rising temperature. This trend may be attributed to the dominant effect of moisture at low temperatures and the dominant effect of thermal softening at high temperatures (Lin et al., 2022; Batuer et al., 2019). At 21℃, the paper exhibited a lower EMC (relative to 1℃), and molecular motion within the fibers had not yet intensified sufficiently to induce softening. Consequently, the elastic modulus reached its

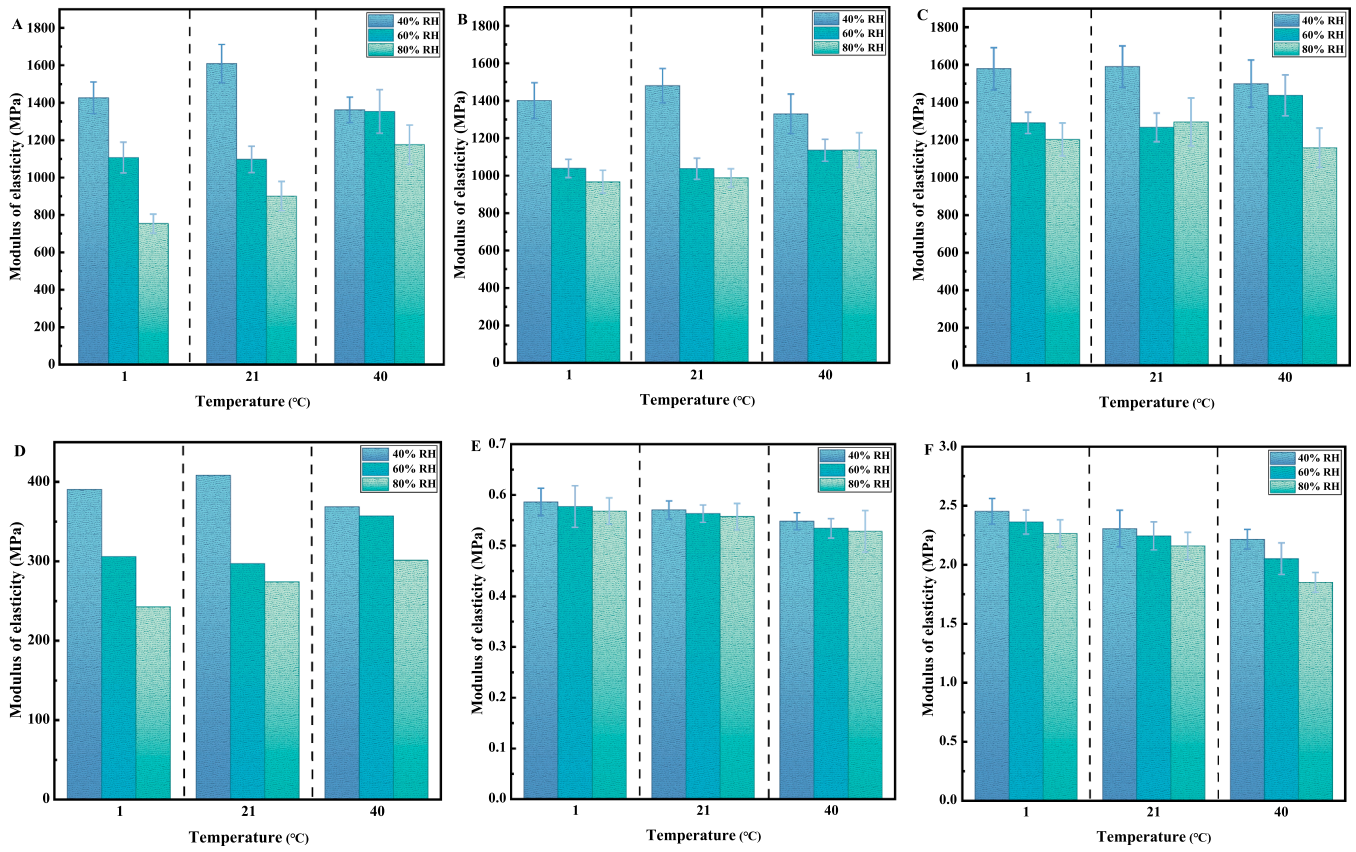

Fig. 2. Elastic modulus of materials under different environmental temperatures and RH. A, Inner liner; B, Fluting; C, Outer liner; D, Equivalent elastic modulus of corrugated board; E, Foam packaging nets; F, Kiwifruit.

maximum value. At 60% RH, the elastic modulus remained stable or slightly decreased with increasing temperature and then increased. This pattern may be attributed to the substantial reduction in EMC at high temperature (40℃) under moderate humidity, which results in drier paper and a weakened moisture-softening effect. At 60% RH, the coupled effects of moisture and temperature were more pronounced at low (1℃) and moderate (21℃) temperatures than at higher temperatures, consistent with the findings of Wang (2018). At 80% RH, the elastic modulus gradually increased with rising temperature. This trend can be attributed to the high EMC of paper under high humidity, where moisture weakening is pronounced and temperature becomes the dominant factor controlling EMC. As temperature increases, EMC decreases, thereby alleviating the adverse effects of moisture (Lin et al., 2022).

Fig. 2E showed that the elastic modulus of the foam net varied significantly with both temperature and RH, decreasing as either factor increased. This trend was attributed to elevated temperatures accelerating polyethylene molecular chain motion, causing the polymer matrix to transition from a glassy to a highly elastic state and macroscopically manifest as softening (Yang et al., 2016). The humidity-driven mechanism arises from water vapor diffusion into the foam pores, where phase transitions disrupt internal thermal equilibrium, while adsorbed trace moisture exerts a slight plasticizing effect on the polymer. Together, these effects reduce the material's stiffness (Chen et al., 2020). Fig. 2F showed that the elastic modulus of kiwifruit varied significantly with both temperature and humidity, decreasing as either factor increased. This behavior was likely driven by a combination of biochemical and physical mechanisms. Elevated temperature activates cell wall-degrading enzymes such as pectinases, accelerating hydrolysis of the cell wall and middle lamella, and leading to tissue disintegration (Llano et al., 2003). Increased humidity effectively limits water loss, maintains turgor pressure, and prevents apparent firmness caused by dehydration, thereby revealing the true softening process driven by enzymatic activity (Mutari & Debbie, 2011; Noichinda et al., 2007; Martínez & Civello, 2008). Furthermore, Du et al. (2019) reported that the elastic modulus of ripe kiwifruit measured by compression tests ranged from 0.2 to 2.4 MPa. The range of elastic modulus obtained from tensile tests in this study (1.8–2.5 MPa) overlapped with that range.

3.2. *Validation of the compression FEM for kiwifruit with CT-NU composite packaging*

Fig. 1H showed the comparison between simulated and experimental compression results of the CT-NU composite packaging under different temperature and humidity conditions. The simulation results showed that the maximum compressive force was 2600 N at 1℃ and 80% RH (simulation 1), 3685 N at 20℃ and 40% RH (simulation 2), 2820 N at 21℃ and 60% RH (simulation 3), 2654 N at 20℃ and 80% RH (simulation 4), and 2813 N at 40℃ and 80% RH (simulation 5). The corresponding experimental result, averaged from five repeated tests, was 2935 N with a standard deviation of 214.4 N. The relative errors between simulations 1–5 and the experimental value were 11.39%, 25.43%, 4.67%, 9.73%, and 4.18%, respectively. It is noteworthy that the simulated values at 20℃ and 60% RH (Simulation 3) and at 40℃ and 80% RH (Simulation 5) closely matched the experimental data. This correspondence was attributed to the actual validation tests being conducted at approximately 21℃ and 60–80% RH, conditions that closely resembled the simulations. These results indicated that the FEM effectively captured the compressive force response under varying environmental conditions. It should be noted that the relatively higher error (25.43%) occurred under the condition of 20℃ and 40% RH, which differs notably from the validation test conditions (21℃, 60–80% RH).

In contrast, when the environmental conditions were similar (Simulation 3: 21℃, 60% RH; Simulation 5: 40℃, 80% RH), the relative errors were much lower (4.67% and 4.18%, respectively). This indicates that the FEM accuracy is highly dependent on the proximity of input material properties to the actual test environment, and the model performs well when conditions are matched. The larger error under dry, moderate-temperature conditions reflects the sensitivity of corrugated board and fruit modulus to humidity, as discussed in Section 3.1.

3.3. FEM of top-load compression for kiwifruit with CT-NU composite packaging

3.3.1. Damage evolution in top-load compression for kiwifruit with CT-NU composite packaging using FE modeling

Fig. 3A-C showed that the 0th step represented the initial state. At 7th step, the perforated edge deformed slightly, increasing stress on adjacent kiwifruit. By 12th step, the edge continued deforming and gradually crushed, raising stress on the contacting kiwifruit while slightly increasing stress on others. At 16th step, the corrugated box was severely crushed and stress on the kiwifruit in contact with the perforated edge reached about 0.25 MPa. At 20th step, stress on kiwifruit touching the top wall and perforated edge peaked at about 0.4 MPa, exceeding the damage threshold. Overall, the progressive deformation of the perforated edge transferred and concentrated stress onto adjacent kiwifruit, causing local stress to surpass the damage threshold.

3.3.2. Sensitivity analysis of FE model for top-load compression

3.3.2.1. Sensitivity of FE simulation of top-load compression to temperature. Under a fixed RH (60%) and compression depth (10 mm), the effect of temperature on the compressive mechanical behavior of the corrugated box and the stress response of the kiwifruit was analyzed using a controlled variable approach. Fig. 4A showed that during the initial loading stage (0–20 s), the compressive force remained below 100 N and the curves at different temperatures nearly overlapped, indicating that this stage mainly reflected contact establishment and that the corrugated board had not yet fully participated in load bearing. In the 20–65 s stage, the compressive force gradually increased to 100–300 N, with the force at 40℃ significantly higher than that at 21℃ and 1℃, indicating that high temperature enhanced the load-transfer capacity of the corrugated board at the same displacement. In the 65–100 s stage, as the displacement approached 10 mm, the compressive force rose sharply to a peak. The peak force was highest at 40℃ (2600–2800 N), followed by 1℃ (2100–2300 N) and lowest at 21℃ (1700–2100 N). This trend is consistent with the variation of the equivalent elastic modulus of the corrugated board with temperature shown in Fig. 2D. At 60% RH, the modulus first remained stable and then increased with temperature. Consequently, the packaging box exhibits higher compressive stiffness and maximum force at higher temperatures.

Fig. 4D showed that during the initial loading stage (0–60 s), stress remained near zero at all three temperatures, indicating that the load was primarily absorbed by the packaging system. As the displacement approached 10 mm, stress increased rapidly and reached a peak, with the fastest growth and highest peak at 40℃, followed by 21℃ and then 1℃. In the later loading stage, stress fluctuated between 0.05 and 0.07 MPa. The increase in temperature led to a higher equivalent elastic modulus of the corrugated box, which raised the reaction force at the same displacement and transmitted stress more effectively through the packaging interface to the fruit. Although stress did not reach the kiwifruit damage threshold under the current conditions, the risk of mechanical damage could increase significantly in actual transport if larger compression displacements occur.

3.3.2.2. Sensitivity of FE simulation of top-load compression to humidity. Under a temperature of 21℃ and a compression depth of 10 mm, the effect of RH (40%, 60%, 80%) on the mechanical response of the system was analyzed. Fig. 4B showed that the compressive force exhibited similar trends at different humidity levels, but the peak values differed markedly. During the 0–20 s stage, the force remained below 100 N and the curves overlapped. In the 20–65 s stage, the compressive force at 40% RH was slightly higher than that at 80% RH, indicating that increased humidity reduced the structural stiffness of the corrugated board. In the 65–100 s stage, the force rose sharply to a peak, which decreased as humidity increased. This was attributed to weakened hydrogen bonding between paper fibers at high humidity, which lowered the equivalent elastic modulus and made the structure more prone to deformation with reduced load-bearing capacity at the same displacement.

Fig. 4E showed that under the same conditions, the maximum stress in the kiwifruit decreased as humidity increased. The peak stress was highest at 40% RH (approximately 0.08 MPa) and gradually decreased at 60% and 80% RH. At low humidity, the corrugated box had higher stiffness and reduced cushioning capacity, causing the load to be transmitted more directly to the kiwifruit. At high humidity, the box stiffness decreased, allowing it to absorb more energy, while the fruit's own modulus decreased and compliance increased, collectively alleviating stress concentration.

3.3.2.3. Sensitivity of FE simulation of top-load compression to compression depth. Under conditions of 21℃ and 60% RH, the effect of compression depth (5, 10, 15 mm) on the mechanical behavior of the system was investigated. Fig. 4C showed that the compressive force of the corrugated box increased significantly with increasing compression depth. During the 0–20 s stage, all curves overlapped and the force remained below 100 N. In the 20–60 s stage, the force increased gradually for the 5 mm condition, while noticeable fluctuations appeared for the 10 mm and 15 mm conditions, indicating progressive participation of the corrugated structure in load bearing. As the displacement reached the target depth, the force rose sharply to about 1000–1200 N for 5 mm, 1800–2100 N for 10 mm, and 2600–2800 N for 15 mm. At larger displacements, the corrugated structure entered a high-deformation range. The equivalent stiffness increased nonlinearly and the reaction force required to maintain the displacement rose significantly.

Fig. 4F showed that the maximum stress in the kiwifruit increased significantly with compression depth. At 5 mm, stress remained below 0.05 MPa and no obvious concentration occurred. At 10 mm, the peak stress approached 0.1 MPa, indicating improved load transfer. At 15 mm, stress rose sharply to about 0.4 MPa, exceeding the kiwifruit damage threshold as determined by the failure stress tests. This indicates that large displacement compression caused pronounced local stress concentration in the fruit and substantially increased the risk of damage.

3.4. FEM of side-load compression for kiwifruit with CT-NU composite packaging

3.4.1. Damage evolution in side-load compression of kiwifruit with CT-NU composite packaging using FE modeling

Fig. 5A-C showed that the step 0 was the initial state. At 7th step, the open edge deformed slightly with minimal effect on the kiwifruit. At 12th step, stress at the open edge increased and the top wall deformed slightly, raising stress in kiwifruit in contact with the loaded side. At 16th step, the box bottom was visibly damaged, and maximum stress appeared along the upper and lower edges of the open side. Kiwifruit in contact reached about 0.65 MPa, exceeding the damage threshold measured in the independent compression tests (Fig. 1D). By 20th step, kiwifruit shifted further, and maximum stress occurred on local surface areas rather than contact regions. This resulted from the collapse of the packaging structure in later stages, where the kiwifruit geometry and internal stress state became dominant under complex displacement,

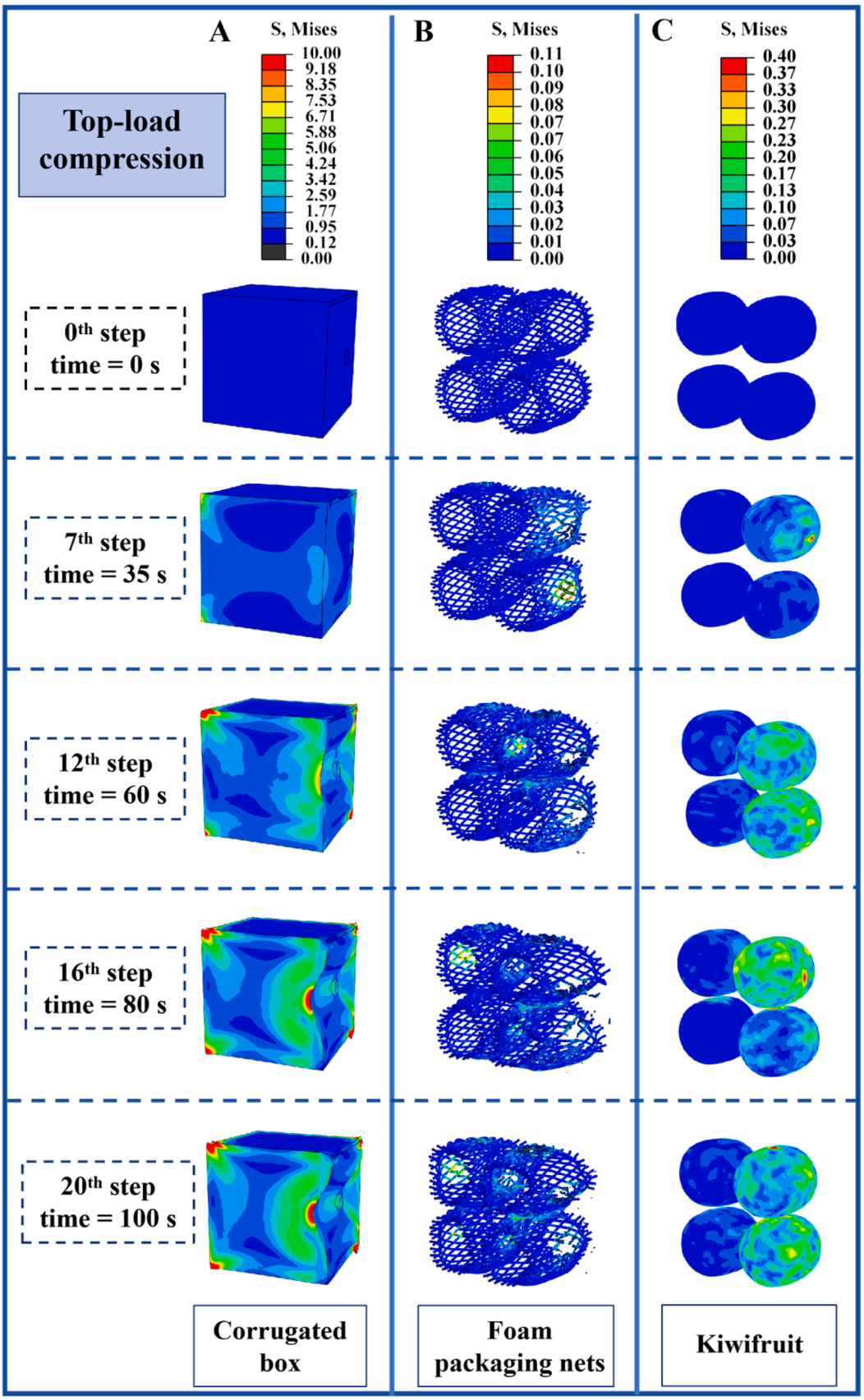

Fig. 3. Von Mises stress distribution cloud diagrams of each component during top-load compression. The Von Mises stress distribution contours of the corrugated box, foam packaging nets, and kiwifruit, respectively under top-load compression (A, B, and C).

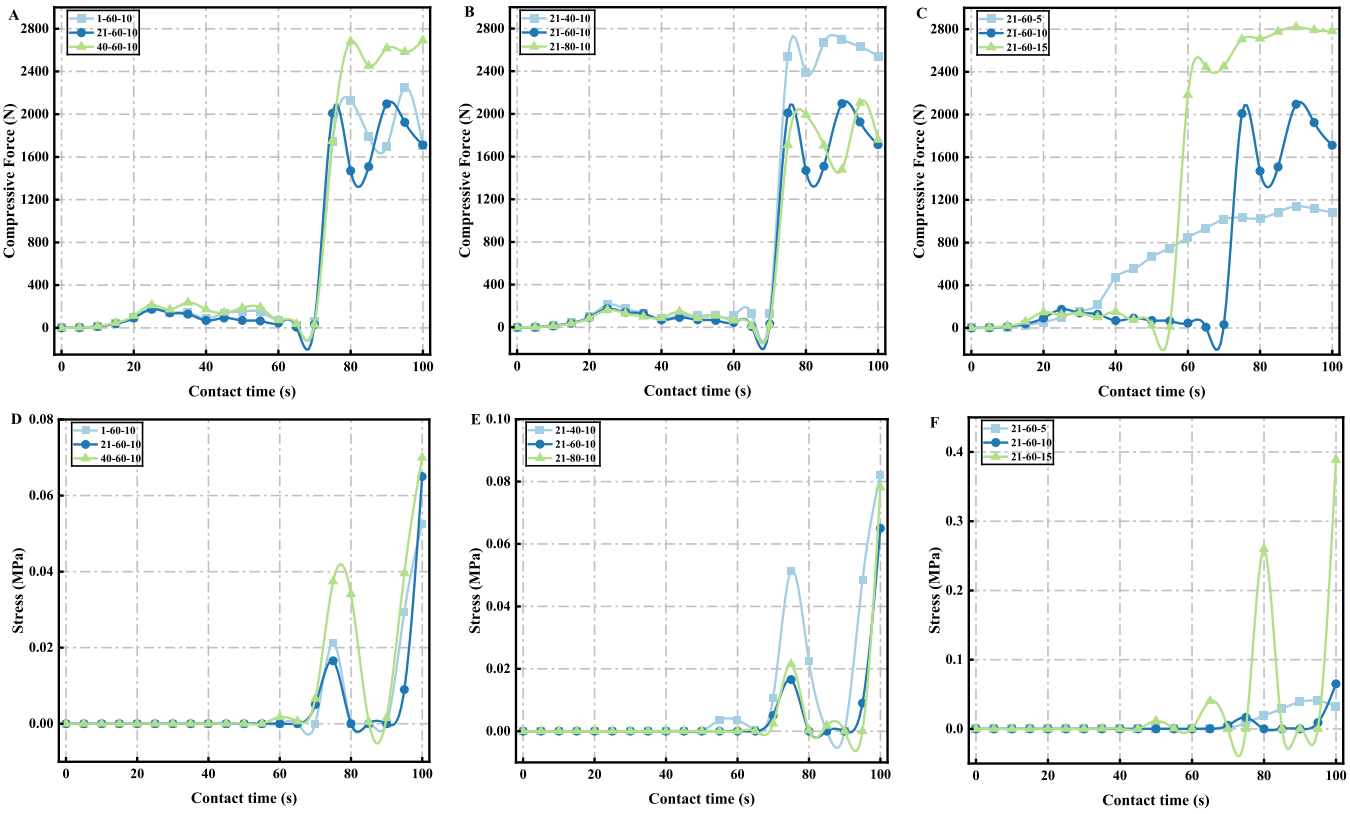

Fig. 4. Sensitivity of the FE model under top-load compression. Sensitivity of the FE model to temperature (A), humidity (B) and compression depth (C) for the compressive force of the corrugated box and for stress response of the kiwifruit (D, E, F) under top-load compression. Note: The labels such as 1–60-10 denote temperature (℃) -relative humidity (%) - compression depth (mm).

leading to local stress concentration on the surface. This shows that side-load compression leads to complex packaging deformation, stress depends on kiwifruit position, and the peak stress may occur away from direct contact.

3.4.2. *Sensitivity analysis of FE model for side-load compression*

3.4.2.1. Sensitivity of FE simulation of side-load compression to temperature. Under fixed humidity of 60% RH and a side-load compression depth of 10 mm, the effects of temperature at 1, 21, and 40℃ on the side mechanical response of the system were examined. Fig. 6A showed that the side-load compression *F-t* curves of the corrugated box largely overlapped during the initial loading stage from 0 to 20 s, with low force levels. This stage mainly reflected structural gap closure, and the influence of temperature was negligible. From 20–60 s, the compression force increased rapidly. Both the slope and magnitude of the force at 40℃ were markedly higher than those at 21℃ and 1℃. This indicates that the equivalent elastic modulus of the corrugated board increased at higher temperature and enhanced the side stiffness of the box. In the later loading stage beyond 60 s, the compression force tended to stabilize under all conditions. The maximum side compressive force at 40℃ was the highest. This finding is consistent with the temperature dependent increase in the elastic modulus of corrugated board.

Fig. 6D showed that the maximum internal stress of kiwifruit was also strongly affected by temperature. During the initial loading stage from 0 to 60 s, the stress remained close to zero, indicating that the load was effectively buffered by the packaging system. After approximately 70–80 s, the stress increased rapidly, with the highest peak at 40℃ exceeding 0.30 MPa, followed by 21℃ at 0.22–0.27 MPa, while 1℃ showed the lowest values. This indicated that, under the same side displacement, higher temperature intensified internal stress concentration in the fruit. The underlying mechanism was that temperature altered the elastic modulus and viscoelastic behavior of the flesh tissue. At higher temperature, mechanical nonlinearity of the tissue became more pronounced, making local stress concentration more likely under displacement constraints. Notably, in some cases the stress peak approached the lower bound of the kiwifruit failure stress at about 0.2 MPa, suggesting that damage risk existed at a side-load compression depth of 10 mm and increased with temperature.

3.4.2.2. Sensitivity of FE simulation of side-load compression to humidity. Under constant temperature of 21℃ and a side-load compression depth of 10 mm, the effect of RH at 40%, 60%, and 80% was investigated. Fig. 6B showed that the side compressive force of the corrugated box at low humidity of 40% RH was consistently higher than that at moderate and high humidity, with a maximum force of about 175–180 N, while it decreased to approximately 120 N and 110 N at 60% and 80% RH, respectively. This indicated that increasing humidity significantly reduced the side-load compression resistance of the box. At low humidity, the corrugated board exhibited a higher elastic modulus and greater structural stiffness, allowing the side walls to form a stable load-bearing framework. At high humidity, material softening and modulus reduction made the corrugated structure more prone to bending, shear, and local collapse, thereby reducing the reaction force at a given displacement. Side-load compression was dominated by sidewall bending and local buckling and was therefore particularly sensitive to changes in material stiffness, making the humidity effect more pronounced than under vertical compression.

Fig. 6E showed that the maximum stress in kiwifruit decreased with increasing humidity. At 40% RH, stress rose sharply at about 60–65 s, reaching a peak of 0.50–0.55 MPa and then stabilized at 0.42–0.45 MPa. At 60% and 80% RH, the stress increase was delayed to about 75–80 s and the peak values were markedly lower at 0.20–0.27 MPa. Under low humidity, the fruit tissue exhibited a higher modulus and limited

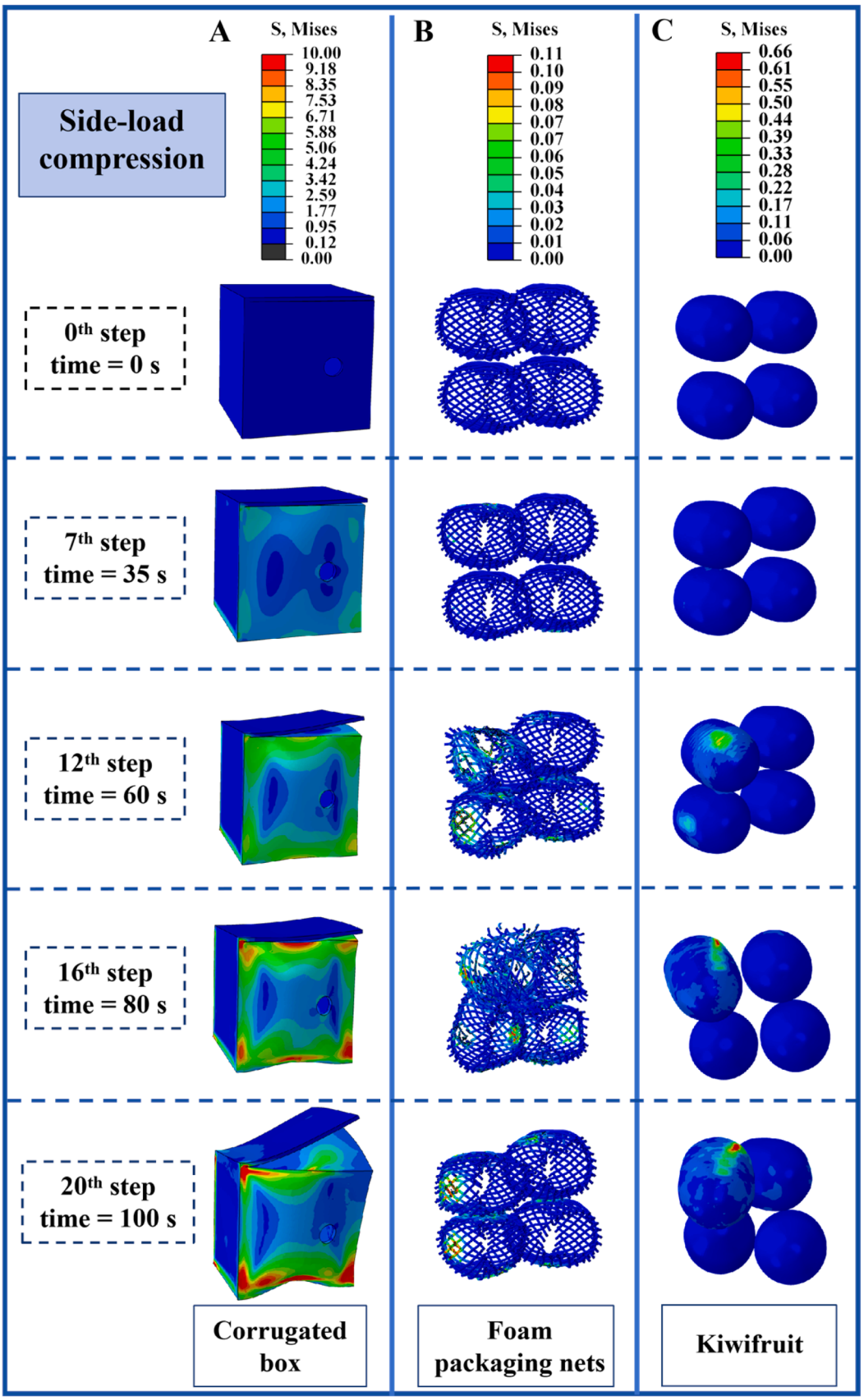

Fig. 5. Von Mises stress distribution cloud diagrams of each component during side-load compression. The Von Mises stress distribution contours of the corrugated box, foam packaging nets, and kiwifruit, respectively under side-load compression (A, B, and C).

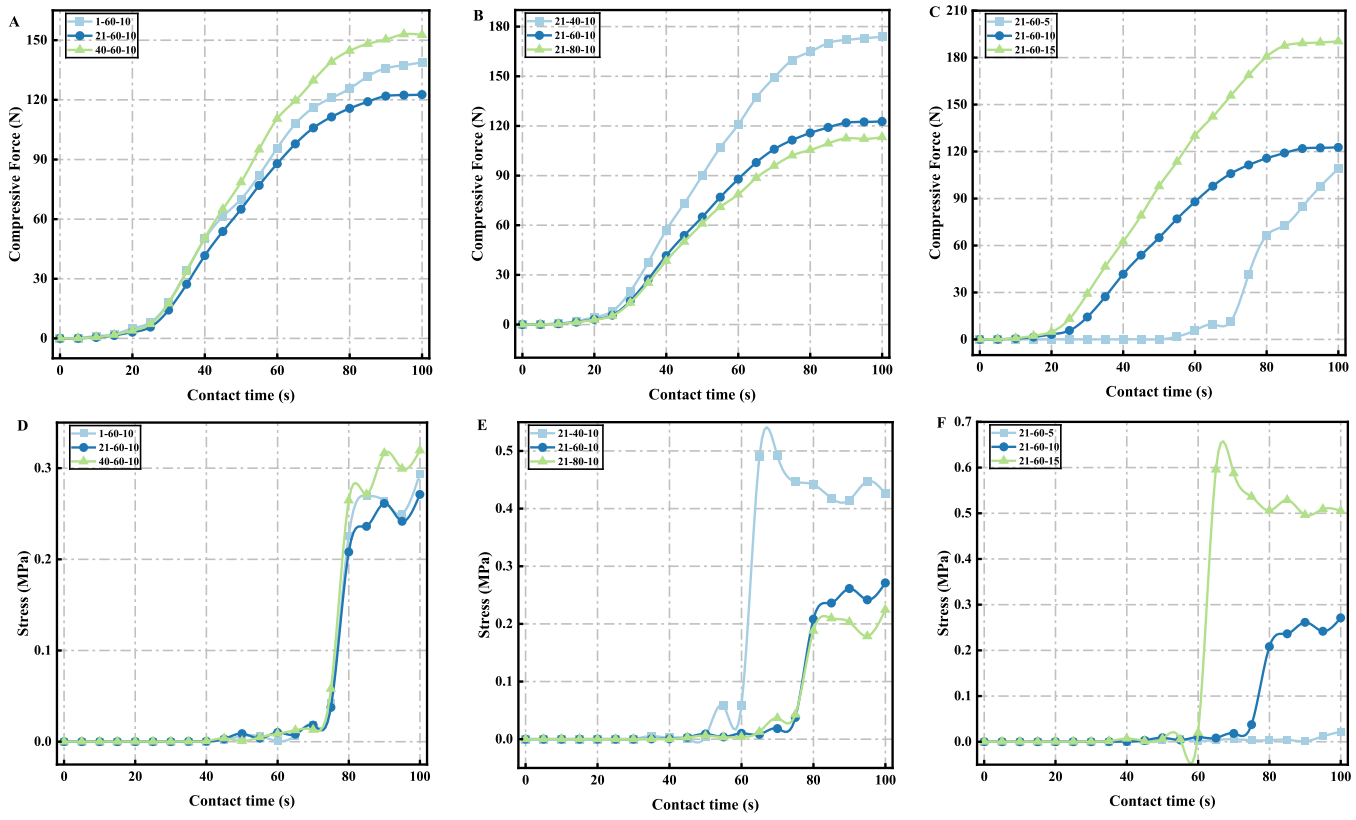

Fig. 6. Sensitivity of the FE model under under side-load compression. Sensitivity of the FE model to temperature (A), humidity (B), and compression depth (C) for the compressive force of the corrugated box and for stress response of the kiwifruit (D, E, F) under side-load compression. Note: The labels such as 1–60-10 denote temperature (℃) - relative humidity (%) - compression depth (mm).

deformability, allowing the load to be transmitted more rapidly and directly into the interior and causing earlier and more severe stress concentration. Under high humidity, the reduced tissue modulus and increased compliance enabled partial energy dissipation through deformation, which delayed stress development and lowered the peak value. Considering the kiwifruit failure stress range of 0.2–0.7 MPa, the stress at 40% RH entered a potential damage range with a higher risk, whereas the risk was relatively lower at moderate and high humidity.

3.4.2.3. Sensitivity of FE simulation of side-load compression to compression depth. Under constant temperature and humidity of 21℃ and 60% RH with consistent material parameters, the effect of side-load compression depth of 5, 10, and 15 mm was investigated. Fig. 6C showed that as the compression depth increased, the slope of the *F-t* curve increased and the maximum side compressive force rose markedly. At 5 mm, the compressive force remained low throughout loading. At 10 mm and 15 mm, the force increased rapidly at an earlier stage. The maximum compressive force at 15 mm was clearly higher than under the other conditions, indicating that larger side displacement induced stronger global bending deformation, crushing of the corrugated medium, and coupled deformation of the liners, which resulted in a nonlinear amplification of the structural reaction force.

Fig. 6F showed that side-load compression depth had a decisive effect on the internal stress of kiwifruit. At 5 mm, stress remained below 0.03 MPa and showed no noticeable localization. At 10 mm, stress rapidly increased to 0.20–0.27 MPa between 75 and 80 s, approaching the lower limit of the damage threshold. At 15 mm, stress sharply rose to 0.60–0.65 MPa between 60 and 65 s and stabilized around 0.50 MPa, reaching the upper range of the damage threshold. At small displacements, the packaging system provided sufficient cushioning. As displacement increased, the cushioning space was exhausted and the load was gradually and then primarily borne by the fruit, causing stress to concentrate sharply. Therefore, side-load compression depth is a critical factor in controlling the mechanical damage risk of kiwifruit and must be strictly limited in packaging design and transport.

3.5. Analysis of resisting compressive damage of kiwifruit with the CT-NU composite packaging

The results of the correlation analysis (Fig. S1 A-B in Supplementary Material) indicated that environmental temperature and relative humidity had a strong correlation with the elastic modulus of the corrugated cardboard box, the EPE foam net, and the kiwifruit. This finding was consistent with the conclusion in Section 3.1 regarding the effect of temperature and humidity on the mechanical properties of materials. Further observation revealed that the three damage indicators, namely the maximum compressive force of the corrugated cardboard box, the maximum stress experienced by the corrugated cardboard box, and the maximum stress experienced by the kiwifruit, were all related to the influence of the elastic modulus of the corrugated cardboard and compression depth.

Given the potential multicollinearity among the independent variables and the intercorrelations among the dependent variables, Pearson correlation analysis, which only presents linear relationships between continuous variables, is insufficient for revealing the relationships between independent and dependent variables. Based on this, the partial least squares regression (PLSR) models were constructed to analyse the ability to resist compressive damage of kiwifruit with the CT-NU composite packaging. Table 2 presented eleven regression models. Models 1–3 described the relationships between temperature and humidity and the elastic modulus of kiwifruit, EPE foam packaging nets, and corrugated board. Models 4–11 used the maximum compressive force of the compression system, the maximum stress of the corrugated box, and the maximum stress of kiwifruit as dependent variables under top-load and

Table 2
Regression models for compression FE analysis of the CT-NU composite packaging and kiwifruit.

Number	Regression analysis model	R^2
1	$E_{Kiwi} = -0.780T - 0.569H$	0.933
2	$E_{EPE} = -0.902T - 0.381H$	0.959
3	$E_{CB} = 0.225\ T - 0.899H$	0.859
4	$F_{Max1} = 0.406E_{CB} + 0.873D$	0.927
5	$\sigma_{Max\text{-}CB1} = 0.297E_{CB} + 0.873D$	0.850
6	$\sigma_{Max\text{-}Kiwi1} = 0.189E_{CB} + 1.166E_{EPE} - 1.201E_{Kiwi} + 0.582D + 0.264T - 0.054H - 0.716F_{Max1} + 0.878\sigma_{Max\text{-}CB1}$	0.736
7	$\sigma_{Max\text{-}Kiwi1} = 0.254E_{CB} + 0.729E_{EPE} - 0.955E_{Kiwi} + 0.723D$	0.612
8	$F_{Max2} = 0.558E_{CB} + 0.695D$	0.793
9	$\sigma_{Max\text{-}CB2} = 0.277E_{CB} + 0.879D$	0.850
10	$\sigma_{Max\text{-}Kiwi2} = 0.764E_{CB} + 0.170E_{EPE} - 0.024E_{Kiwi} + 0.117D - 0.098\ T + 0.615H - 0.050F_{Max2} + 0.724\sigma_{max\text{-}CB2}$	0.786
11	$\sigma_{Max\text{-}Kiwi2} = 0.462E_{CB} + 0.659E_{EPE} - 0.606E_{Kiwi} + 0.719D$	0.692

Note: E_{Kiwi} - elastic modulus of kiwifruit, MPa; E_{EPE} - elastic modulus of EPE foam net, MPa; E_{CB} - elastic modulus of corrugated cardboard, MPa; D - depth of compression, mm; T - temperature, ℃; H - humidity, RH%; F_{Max1} - the maximum compressive force from the top-loading compression FEA, N; F_{Max2} - the maximum compressive force from the side-loading compression FEA, N; $\sigma_{Max\text{-}CB1}$ - the maximum stress in the corrugated box from top-loading compression FEA, MPa; $\sigma_{Max\text{-}CB2}$ - the maximum stress in the corrugated box from side-loading compression FEA, MPa; $\sigma_{Max\text{-}Kiwi1}$ - the maximum stress in the kiwifruit from top-compression FEA, MPa; $\sigma_{Max\text{-}Kiwi2}$ - the maximum stress in the kiwifruit from side-compression FEA, MPa.

side-load FE simulations of the CT-NU composite packaging with kiwifruit. Except for the models of maximum kiwifruit stress, all models showed R^2 values greater than 0.79, indicating good fitting performance.

The regression models showed that the maximum compressive force was positively correlated with the corrugated box modulus and compression depth ($p < 0.05$). Each 1 MPa increase in modulus raised F_{Max1} by 0.406 N and F_{Max2} by 0.558 N. Each 1 mm increase in compression depth increased F_{Max1} by 0.873 N and F_{Max2} by 0.695 N. Temperature and humidity also had significant effects on the maximum compressive force, since they altered material elastic moduli and thereby influenced the compression response. Under both top-loading and side-loading conditions, compression depth exerted the strongest influence on the maximum compressive force, with beta weight coefficient of 0.873 and 0.879, respectively (Fig S2 D-H in Supplementary Material). Moreover, the VIP analysis also identified compression depth as a key influencing factor (VIP > 1).

Compression depth and the elastic modulus strongly influenced the maximum stress of the corrugated box ($p < 0.05$). A 1 MPa increase in modulus raised the maximum stress by about 0.297 MPa for top compression and 0.277 MPa for side compression. A 1 mm increase in compression depth increased stress by about 0.873 MPa and 0.879 MPa for top and side compression, respectively. Maximum stress was positively correlated with compressive force and displacement, with R^2 of 0.867 and 0.872 for top and side compression, indicating that higher modulus amplified the compressive response and stress. Compression depth ranked as the most influential variable, with beta weight coefficient of 0.873 (top-loading) and 0.695 (side-loading) (Fig S2 E-I). VIP values further confirmed compression depth as a critical factor (VIP > 1), followed by the elastic modulus of the corrugated box.

The maximum stress in kiwifruit under top-load and side-load compression was mainly influenced by the corrugated box's maximum stress, the maximum compressive force, and compression depth. A 1 MPa increase in corrugated box stress raised kiwifruit stress by 0.878 MPa under top compression and 0.724 MPa under side compression. A 1 N increase in maximum compressive force increased kiwifruit stress by 0.716 MPa and 0.050 MPa, while a 1 mm increase in compression depth raised stress by 0.582 MPa and 0.117 MPa for top and side compression, respectively. Kiwifruit elastic modulus had a smaller effect under side compression. Enhancing the elastic modulus of the corrugated box is crucial for improving packaging protection. Fig S2 F-J (beta weight coefficient) presented factors that showed relatively large effects included the elastic modulus of the kiwifruit itself, the elastic modulus of the EPE foam net, the maximum stress of the corrugated box, the maximum compressive force, and the compression depth. According to the VIP values, the maximum stress of the corrugated box, the maximum compressive force, and the compression depth were key influencing factors (VIP > 1). In addition, under the side-loading condition, the elastic modulus of the corrugated board also yielded a VIP greater than 1.

Since box stress and compressive force are intermediate variables influenced by compression depth and box modulus, the simplified model used only independent variables. Compression depth, box modulus, and EPE foam modulus were key factors affecting kiwifruit stress and damage risk. Both the beta weight coefficients and VIP values indicated that compression depth was the most influential factor on the maximum stress of the kiwifruit (Fig S2 G-K).

4. Conclusion

This study systematically evaluated the protective performance of CT-NU composite packaging under simulated express delivery conditions. The results showed that temperature and humidity significantly affected the mechanical properties of both the packaging materials and kiwifruit. The elastic modulus of corrugated board decreased with increasing humidity, while the modulus of kiwifruit and the EPE foam packaging nets decreased significantly as temperature and humidity rose. In terms of compression damage, local stress in kiwifruit exceeded its damage threshold in the simulations at 15 mm compression under both top-load and side-load compression. Compression depth and the elastic modulus of the corrugated board were the dominant factors affecting system maximum compressive force and fruit stress. The developed regression models showed good predictive capability under the tested conditions, effectively capturing the mechanical responses across different conditions. This study is the first to perform dual-mode compression simulations of CT-NU composite packaging while incorporating coupled environmental factors. The FEM showed validation errors ranging from 4.18% to 25.43%, with the largest error (25.43%) occurring under environmental conditions (20°C, 40% RH) that differed most from the validation setup, while errors were below 10% under matched conditions. This provides a preliminary theoretical basis and a validated simulation tool under similar compression conditions for optimizing kiwifruit protective packaging, reducing transport losses, and extending fruit shelf life.

It should be noted that the elastic modulus of kiwifruit used in the finite element simulations was derived from tensile tests, whereas actual compressive loads would ideally be simulated using compression-derived moduli. A comparison with Du et al. (2019) shows that the numerical ranges of compressive and tensile elastic moduli overlap. More importantly, the failure stress used as the damage criterion was obtained from independent compression tests on whole fruit (Fig. 1D), ensuring a realistic damage threshold. The FEM was validated against physical compression tests of the complete CT-NU packaging system (Section 3.2), with relative errors ranging from 4.18% to 25.43%. However, the simulations were performed under idealized quasi-static loading conditions with simplified material assumptions (e.g., isotropy of corrugated board) and did not account for dynamic vibrations or impact loads that may occur in actual express transport. Future work should include experimental validation under dynamic loading and field tests, as well as direct measurement of the compressive elastic modulus of kiwifruit for improved prediction accuracy.

CRediT authorship contribution statement

Fauconnier Marie-Laure: Writing – review & editing. **Minggang Wang:** Resources, Investigation. **Clément Burgeon:** Writing – review & editing, Conceptualization. **Hao Liu:** Resources. **Yun Yang:** Writing – review & editing. **Jie Hao:** Writing – original draft, Validation, Resources, Project administration, Investigation. **Zhinan Wu:** Formal analysis.

Declaration of Competing Interest

We declare that none of the work contained in this manuscript is published in any language or currently under consideration at any other journal, and there are no conflicts of interest to declare. All authors have contributed to, read, and approved this submitted manuscript in its current form.

Acknowledgments

This work was supported by Northwest A&F University Doctoral Candidates' Independent Innovation Research Project Funding (2025KYCXZ25).

Appendix A. Supporting information

Supplementary data associated with this article can be found in the online version at doi:10.1016/j.fpsl.2026.101769.

Data availability

Data will be made available on request.

References

Alique, R., Zamorano, J. P., Martínez, M. A., & Alonso, J. (2005). Effect of heat and cold treatments on respiratory metabolism and shelf-life of sweet cherry, type picota cv "Ambrunés. *Postharvest Biology and Technology, 35*(2), 153–165. https://doi.org/10.1016/j.postharvbio.2004.07.003

Allaoui, S., Aboura, Z., & Benzeggagh, M. L. (2009). Effects of the environmental conditions on the mechanical behaviour of the corrugated cardboard. *Composites Science and Technology, 69*(1), 104–110. https://doi.org/10.1016/j.compscitech.2007.10.058

Ambaw, A., Mukama, M., Fadiji, T., & Opara, U. L. (2022). Fresh fruit packaging design verification through virtual prototyping technique. *Food Packaging and Shelf Life, 32*, Article 100858. https://doi.org/10.1016/j.fpsl.2022.100858

An, X., Zhu, P., Li, Z., Fadiji, T., & Wani, A. A. (2023). Effect of expanded polyethylene (EPE) foam packing net design on the mechanical damage resistance of strawberry fruit during transportation. *Food Packaging and Shelf Life, 40*, Article 101193. https://doi.org/10.1016/j.fpsl.2023.101193

Batuer, A., Chen, D., Yin, L., & Feng, Y. (2019). Correlation between mechanical properties and thermochemical behaviours of waste papers in their early devolatilization stage. *Journal of Analytical and Applied Pyrolysis, 137*, 128–137. https://doi.org/10.1016/j.jaap.2018.11.017

Chen, R., Wang, Z., Li, S., & Du, H. (2020). A novel degradation mechanism of the elastic modulus of wet polymer substrates under nanoindentation. *Soft Matter, 16*(21), 5009–5019. https://doi.org/10.1039/d0sm00645a

Csavajda, P., & Böröcz, P. (2021). Effect of temperature changes on the vibration transmissibility of XPE and PE packaging cushioning material. *Applied Sciences, 11*(2), 482. https://doi.org/10.3390/app11020482

Du, D., Wang, B., Wang, j, Yao, F., & Hong, X. (2019). Prediction of bruise susceptibility of harvested kiwifruit (Actinidia chinensis) using finite element method, 36-34 *Postharvest Biology and Technology, 152*. https://doi.org/10.1016/j.postharvbio.2019.02.013.

Fadiji, T., Ambaw, A., Coetzee, C. J., Berry, T. M., & Opara, U. L. (2018). Application of finite element analysis to predict the mechanical strength of ventilated corrugated paperboard packaging for handling fresh produce. *Biosystems Engineering, 174*, 260–281. https://doi.org/10.1016/j.biosystemseng.2018.07.014

Fadiji, T., Coetzee, C., Pathare, P., & Opara, U. L. (2016). Susceptibility to impact damage of apples inside ventilated corrugated paperboard packages: Effects of package design. *Postharvest Biology and Technology, 111*, 286–296. https://doi.org/10.1016/j.worlddev.2025.107118

Fadiji, T., Coetzee, C., & Opara, U. L. (2016). Compression strength of ventilated corrugated paperboard packages: Numerical modelling, experimental validation and effects of vent geometric design. *Biosystems Engineering, 151*, 231–247. https://doi.org/10.1016/j.biosystemseng.2016.09.010

Fernando, I., Fei, J., Stanley, R., & Enshaei, H. (2018). Measurement and evaluation of the effect of vibration on fruits in transit-Review. *Packaging Technology and Science, 31*(11), 723–738. https://doi.org/10.1002/pts.2409

Hao, J., Dong, F., Li, Y., Wang, S., Cui, J., Liu, S., & Lv, Y. (2023). Quantification of polycyclic aromatic hydrocarbons in roasted Tan lamb using fluorescence hyperspectral imaging technology. *Journal of Food Composition and Analysis, 124*, Article 105646. https://doi.org/10.1016/j.jfca.2023.105646

Hao, J., Qiao, P., Wang, J., Wang, M., Li, Z., Tang, W., & Fauconnier, M. (2025). Advanced packaging technology for fresh fruit: From anti-damage and preservation to intelligent monitoring. *Trends in Food Science & Technology, 166*, Article 105369. https://doi.org/10.1016/j.tifs.2025.105369

Kalita, N., Saxena, P., & Talha, M. (2021). Influence of stiffeners for improving the compressive strength of ventilated corrugated packages using finite element modelling technique. *Sustainability, 13*(24), 13926. https://doi.org/10.3390/su132413926

Lang, K., & Su, M. (2022). Equivalent orthotropic model for corrugated plates based on simplified constitutive relation. *Heliyon, 8*, Article e11264. https://doi.org/10.1016/j.heliyon.2022.e11264

Li, Z., & Thomas, C. (2014). Quantitative evaluation of mechanical damage to fresh fruits. *Trends in Food Science & Technology, 35*(2), 138–150. https://doi.org/10.1016/j.tifs.2013.12.001

Li, X., Wang, J., Huang, C., Gao, D., Lu, G., Lu, L., & Wang, Z. (2018). Mathematical models for predicting the quasi-static stress characteristics of corrugated paperboard with sinusoidal core along the longitudinal compression. *International Journal of Mechanical Sciences, 149*, 136–149. https://doi.org/10.1016/j.ijmecsci.2018.07.028

Lin, B., Auernhammer, J., Schäfer, J., Meckel, T., Stark, R., Biesalski, M., & Xu, B. (2022). Humidity influence on mechanics of paper materials: Joint numerical and experimental study on fiber and fiber network scale. *Cellulose, 29*(2), 1129–1148. https://doi.org/10.1007/s10570-021-04355-y

Lin, M., Fawole, O. A., Saeys, W., Wu, D., Wang, J., Opara, U. L., Nicolai, B., & Chen, K. (2023). Mechanical damages and packaging methods along the fresh fruit supply chain: A review. *Critical Reviews in Food Science and Nutrition, 63*(30), 10283–10302. https://doi.org/10.1080/10408398.2022.2078783

Lin, M., Gao, Z., Wang, X., Huo, H., Mao, J., Gong, X., Chen, L., Ma, S., & Cao, Y. (2024). Eco-friendly managements and molecular mechanisms for improving postharvest quality and extending shelf life of kiwifruit: A review. *International Journal of Biological Macromolecules, 257*, Article 128450. https://doi.org/10.1016/j.ijbiomac.2023.128450

Liu, H., Han, X., Fadiji, T., Li, Z., & Ni, J. (2022). Prediction of the cracking susceptibility of tomato pericarp: Three-point bending simulation using an extended finite element method. *Postharvest Biology and Technology, 187*, Article 111876. https://doi.org/10.1016/j.postharvbio.2022.111876

Llano, K. M., Haedo, A. S., Gerschenson, L. N., & Rojas, A. M. (2003). Mechanical and biochemical response of kiwifruit tissue to steam blanching. *Food Research International, 36*(8), 767–775. https://doi.org/10.1016/S0963-9969(03)00071-1

Marin, G., Srinivasa, P., Nygårds, M., & Östlund, S. (2021). Experimental and finite element simulated box compression tests on paperboard packages at different moisture levels. *Packaging Technology and Science, 34*(4), 229–243. https://doi.org/10.1002/pts.2554

Martínez, G. A., & Civello, P. M. (2008). Effect of heat treatments on gene expression and enzyme activities associated to cell wall degradation in strawberry fruit. *Postharvest Biology and Technology, 49*(1), 38–45. https://doi.org/10.1016/j.postharvbio.2008.01.013

Meng, C. Y. (2010). Analysis of the influence of corrugated shape on mechanical properties of corrugated board. *China National Knowledge Infrastructure (CNKI)*. Wuhan University of Technology (In Chinese).

Mutari, A., & Debbie, R. (2011). The effects of postharvest handling and storage temperature on the quality and shelf of tomato. *African Journal of Food Science, 5*(7), 446–452.

Noichinda, S., Bodhipadma, K., Singkhornart, S., & Ketsa, S. (2007). Changes in pectic substances and cell wall hydrolase enzymes of mangosteen (Garcinia mangostana) fruit during storage. *New Zealand Journal of Crop and Horticultural Science, 35*(2), 229–233. https://doi.org/10.1080/01140670709510189

Opara, U. L., & Fadiji, T. (2018). Compression damage susceptibility of apple fruit packed inside ventilated corrugated paperboard package. *Scientia Horticulturae, 227*, 154–161. https://doi.org/10.1016/j.scienta.2017.09.043

Opara, U. L., & Pathare, P. B. (2014). Bruise damage measurement and analysis of fresh horticultural produce-a review. *Postharvest Biology and Technology, 91*, 9–24. https://doi.org/10.1016/j.postharvbio.2013.12.009

Palsson, H., & Sandberg, E. (2021). Packaging paradoxes in food supply chains: Exploring characteristics, underlying reasons and management strategies. *International Journal of Physical Distribution & Logistics Management, 52*(11), 25–52. https://doi.org/10.1108/IJPDLM-09-2019-0270

Słupska, M., Kuprianiuk, S., Stopa, R., & Figiel, A. (2026). Finite element modeling of apple tissue mechanics: A comparative study of elastic and elastoplastic behavior across ripening stages. *Journal of Food Engineering, 402*, Article 112696. https://doi.org/10.1016/j.jfoodeng.2025.112696

Wang, D. (2018). Elastic modulus prediction of corrugating medium under different temperature and relative humidity. In *IOP conference series. Materials Science and Engineering, 439* p. 42043). https://doi.org/10.1088/1757-899X/439/4/042043

Xia, M., Zhao, X., Wei, X., Guan, W., Wei, X., Xu, C., & Mao, L. (2020). Impact of packaging materials on bruise damage in kiwifruit during free drop test. *Acta Physiologiae Plantarum, 42*(7), 119. https://doi.org/10.1007/s11738-020-03081-5

Yang, P., Hao, J., Li, Z., Tchuenbou-Magaia, F., & Ni, J. (2024). Wind disturbance-based tomato seedlings growth control. *Biosystems Engineering, 243*, 82–92. https://doi.org/10.1016/j.biosystemseng.2024.05.007

Yang, Q., Chen, X., He, Z., Lan, F., & Liu, H. (2016). The glass transition temperature measurements of polyethylene: Determined by using molecular dynamic method. *RSC Advances, 6*(15), 1126–1253. https://doi.org/10.1039/C5RA21115H

Yu, J., Qiang, H., Shi, M., Li, Z., Fadiji, T., Wani, A. A., & Burgeon, C. (2025a). Investigation on the protection ability of two commonly packaging methods to apples during express transportation. *Food Packaging and Shelf Life, 48*, Article 101475. https://doi.org/10.1016/j.fpsl.2025.101475

Yu, J., Qiang, H., Tang, W., Tchuenbou-Magaia, F., Marie-Laure, F., Burgeon, C., Wang, M., Liu, Y., & Li, Z. (2025b). Analysis of protective ability of pomelo peel against impact damage to apple for cushioning packaging design. *Food Packaging and Shelf Life, 52*, Article 101644. https://doi.org/10.1016/j.fpsl.2025.101644

Yu, J., Wang, M., Li, Z., Tchuenbou-Magaia, F., Wani, A. A., Zhu, P., Fadiji, T., & Liu, Y. (2024). Preserving freshness:Innovations for fresh-eating fruit distribution and damage prevention - a review. *Food Packaging and Shelf Life, 44*, Article 101323. https://doi.org/10.1016/j.fpsl.2024.101323

Zhu, Y., Zhu, L., Guo, W., Han, Z., Wang, R., Zhang, W., Yuan, Y., Gao, J., & Liu, S. (2024). Multiscale static compressive damage characteristics of kiwifruit based on the finite element method. *Foods, 13*(5), 785. https://doi.org/10.3390/foods13050785